HHS Public Access

Author manuscript

Trends Biochem Sci. Author manuscript; available in PMC 2016 September 01.

Published in final edited form as:

Trends Biochem Sci. 2015 September ; 40(9): 526–534. doi:10.1016/j.tibs.2015.07.002.

Deciphering Voltage-gated Na^+ and Ca^{2+} Channels By Studying Prokaryotic Ancestors

William A. Catterall[1] and **Ning Zheng**[1,2]

[1]Department of Pharmacology, Box 357280, University of Washington, Seattle, WA 98195

[2]Howard Hughes Medical Institute, Box 357280, University of Washington, Seattle, WA 98195

Abstract

Voltage-gated sodium (Na_V) and calcium (Ca_V) channels are involved in electrical signaling, contraction, secretion, synaptic transmission, and other physiological processes activated in response to depolarization. Despite their physiological importance, the structures of these closely related proteins have remained elusive because of their size and complexity. Bacterial Na_V channels have structures analogous to a single domain of eukaryotic Na_V and Ca_V channels and are their likely evolutionary ancestor. In this article, we review recent work that has led to new understanding of Na_V and Ca_V channels through high-resolution structural studies of their prokaryotic ancestors. New insights into their voltage-dependent activation and inactivation, ion conductance, and ion selectivity provide realistic structural models for the function of these complex membrane proteins at the atomic level.

Keywords

voltage-gated sodium channel; voltage-gated calcium channel; NaChBac; NavAb; voltage sensor; selectivity filter; slow inactivation

Voltage-gated Na_V and Ca_V channels and their bacterial ancestors

Voltage-gated Na_V channels (Na_Vs) initiate action potentials in excitable cells and are crucial for electrical signaling from bacteria to man [1]. Voltage-gated Ca_V channels (Ca_Vs) are activated by depolarization during action potentials, and Ca^{2+} entry through them initiates synaptic transmission, muscle contraction, hormone secretion, and many other biochemical and physiological processes [2, 3]. These channels are thought to share similar voltage-dependent activation and inactivation processes, whose structural basis is fundamental for electrical signaling. Moreover, how these channels can rapidly and selectively conduct Na^+ or Ca^{2+} ions in response to changes of the electrical membrane potential is a crucial question in biology.

Corresponding authors: Catterall, W. A. (wcatt@uw.edu), Zheng, N. (nzheng@uw.edu).

Mammalian Na_V channels are complexes of a large α subunit of 260 kDa and smaller β subunits of 30-40 kDa [4]. cDNA encoding the pore-forming α subunits is sufficient for expression of functional Na_V channels, whereas the β subunits enhance expression, modulate Na_V channel gating, and serve as cell adhesion molecules (reviewed in [5, 6]). Na_V channel α subunits are polypeptides of approximately 2000 amino acid residues organized into four homologous domains, each containing six transmembrane segments (Figure 1a) [5, 6]). Each homologous domain consists of two functional modules: a voltage-sensing module (VSM) composed of the S1-S4 segments, and a pore-forming module (PM) composed of the S5 and S6 segments and the P loop between them (Figure 1a).

Mammalian Ca_V channels are also multi-subunit complexes [3]. They have a central, pore-forming α1 subunit that is analogous in structure and function to the Na_V channel α subunit. The α1 subunit is associated with an intracellular β subunit, a membrane-associated α2δ disulfide-linked complex, and a transmembrane γ subunit, all of which are involved in channel regulation but not in voltage-dependent gating or ion conductance. Analysis of the pore-forming sequences of the 143 voltage-gated ion channels and their relatives in the human genome predicted a common core domain composition with many key conserved structural elements. These conserved features led to the proposal that Na_V and Ca_V channels derive from a common ancestor and have a similar structural basis for their function [7]. Despite their high biological significance, the sheer sizes and complex transmembrane architectures of these channel proteins have posed a major challenge for structural and mechanistic analyses of their functions.

The unexpected discovery of the bacterial Na_V channel NaChBac was a landmark in ion channel research [8]. The sequence of NaChBac is analogous to one domain of the eukaryotic Na_V or Ca_V channel, and it functions as a homotetramer (Figure 1b) [8]. Orthologs of NaChBac are found in gram-positive and gram-negative eubacteria and in archaea, suggesting a truly ancient origin [8]. Although its amino acid sequence in the pore region is closer to Ca_V channels, NaChBac selectively conducts Na^+. These properties further confirmed its identity as an ancestor of both mammalian Na_V or Ca_V channels. The bacterial Na_V channels are ‘minimalist’ in structure, as they have a VSM and PM but no large intracellular and extracellular linkers. This minimalist structure makes them ideally suited for structural studies of the conserved core functions of Na_V and Ca_V channels. This article reviews the mechanistic insights into the conserved core functions of Na_V and Ca_V channels gained from structural analyses of the NaChBac family of bacterial ion channels.

The first glimpse of Na_V channel structure

One decade after identification of NaChBac, the X-ray crystal structure of its ortholog from *Arcobacter butzleri* (Na_VAb) was determined at 2.7 Å resolution [9], opening the way to understanding Na_V channel structure and function at the atomic level. The Na_VAb structure revealed a homotetrameric architecture, in which four subunits pack in a symmetric manner, giving rise to a functional channel with a central ion-conducting pore (Figure 2a). The four S5 and S6 helices and the P loops form the pore, which is surrounded by the form VSM composed of the S1-S4 helices. Interestingly, although the VSM of each subunit is coupled to the pore via an α-helical S4-S5 linker, its closest noncovalent contacts are with the S5

helix of its neighboring subunit (Figure 2a, 2b). The S4-S5 linker helix of each subunit also directly intersects the S5 and S6 helices of the adjacent subunit. Such a tightly interlocked subunit arrangement suggests that the four VSMs cooperatively control concerted opening of the pore.

The Na_VAb structure unveiled the detailed anatomy of a Na_V pore. The Na_VAb pore consists of an external vestibule, a narrow ion selectivity filter, a spacious water-filled central cavity, and an activation gate in closed conformation at the inner end of the S6 helices, completely sealing off the ion-conduction pathway (Figure 2c, 2d). Because Na_VAb activates at very negative membrane potentials, it is not surprising that the channel was crystallized with an activated VSMs at the 0-mV potential in a protein crystal. The combination of four activated VSMs and a closed pore strongly suggests that the Na_VAb Ile217Cys mutant used for high-resolution structure determination was crystallographically trapped in a pre-open state, which is a required intermediate for a homotetrameric channel that opens in a single concerted transition (see Glossary). The Na_VAb crystal structure ended the long wait for a high-resolution view of a voltage-gated Na_V channel and heralded further analyses of the structural underpinnings of both Na_V and Ca_V channel functions.

Prokaryotic Na_V channel structure in greater detail

Following the Na_VAb structure, an explosion of structural studies of bacterial Na_V channels provided additional insights into the structural basis of channel functions. Wild-type Na_VAb (Na_VAb-WT) succumbed to crystallographic analysis, which fortuitously captured the channel in two slow-inactivated states (see below and [10]). Structure determination of Na_VRh from *Richettsiales sp. HIMB114* offered an independent view of a Na_V channel, also captured in a slow-inactivated state [11]. The activated VSMs of Na_VRh wrap around the central pore at a different angle and the S4 segment has moved further outward than in Na_VAb, implying a considerable degree of flexibility in VSM-pore interactions (Figure 2e). Recently, electron crystallography was used to determine the overall architecture of a third NaChBac family member from *Caldalkalibacillus thermarum* (Na_VCt). Despite relatively low 9Å resolution, two distinguishable conformations of Na_VCt were readily recognized [12], marked by different degrees of openness of the S6 intracellular activation gate (see Glossary) and, surprisingly, by a partially blurred S4-S5 linker helix.

The modular architecture of bacterial Na_V channels allows their S5-S6 segments to assemble into a functional pore in the absence of VSMs. Such a strategy has been adopted to obtain crystal structures of two pore-only bacterial channels from *Magnetococcus sp.* (Na_VMs [13]) and *Alkalilimnicola ehrlichei* (Na_VAe1 [14, 15]). The Na_VMs pore shares nearly an identical selectivity filter with Na_VAb, but adopts an open conformation at the intracellular S6 activation gate (Figure 2f, 2g). Superposition analysis of the S6 helix in Na_VMs and Na_VAb indicates that gate opening is mediated by a slight rotation about a single residue in the middle of the S6 helix in close proximity to a strictly conserved Asn residue facing directly toward the S4-S5 linker. By capturing the partially or fully open pore, the Na_VMs pore structures gave additional insight into structural mechanisms of pore opening and closing [16]. Based on these structures, VSM activation may open the activation gate by splaying the S6 helix at a central hinge residue, as in the Na_VMs structure. However, the absence of

the interacting S4-S5 linker may alter conformational movement of the S6 segment in the pore-only Na_VMs structure relative to the complete channels with VSMs. Future studies are needed to validate this mechanism.

In contrast to Na_VMs, the pore-only structure of NavAe1 shows a closed activation gate [15], as in Na_VAb. A unique observation from this structure is the well-resolved C-terminal tail extending from the S6 helix in a four-helix bundle that would project into the cytosol in a bacterial cell (Figure 2h) [15]. This C-terminal sequence is found in many bacterial Na_V channels. Mutational and structural analyses of this sequence have established its functional role in assembly, gating, and inactivation [12, 15, 18, 19].

Led by Na_VAb, the bacterial NaChBac family Na_V channel structures not only revealed the overall architecture of a Na_V channel in different functional states, but also offered detailed insights into the structural mechanisms underlying their essential functions. These include voltage sensing, channel inactivation, and ion selectivity and conductance, which are highlighted next.

Voltage-dependent activation

Voltage-dependent activation of Na_V channels depends on voltage-driven transmembrane movement of gating charges (see Glossary) in the S4 segment [1]. This charge movement was first detected as a small capacitive gating current in voltage clamp studies [20, 21]. The S4 transmembrane segments contain 4-8 repeated motifs of a positively charged amino acid residue (usually arginine) flanked by two hydrophobic residues. They were proposed to carry the gating charges in the *sliding helix* model of voltage sensing [5]. This conceptual model was placed on a solid structural foundation by molecular modeling using the Rosetta Membrane algorithm together with structural information on the $K_V1.2$ channel [22] and the Na_VAb channel [17]. Extensive structure-function studies now provide strong support for this model [23], and a consensus mechanism for voltage sensor function based on the *sliding helix* model has emerged [24].

The high-resolution structures of the VSMs of $K_V1.2$ and Na_VAb channels revealed the functional conformation of their voltage sensors [9, 25-27]. The S4 transmembrane segment arrays the gating charges across the membrane. Three gating charges (R1-R3 in Na_VAb) are exposed to the external solution and interact with negatively charged and hydrophilic amino acid side chains in the Extracellular Negative Cluster (ENC) in the S1-S3 segments (Figure 3) [9]. The fourth conserved gating charge (R4 in Na_VAb) interacts with negatively charged amino acid side chains in the Intracellular Negative Cluster (INC) [9]. Between the third and fourth gating charges, the highly conserved Hydrophobic Constriction Site (HCS) seals the voltage sensor and prevents transmembrane movement of water and ions [9]. In the context of the *sliding helix* model, the S4 segment is thought to move through the HCS in response to changes in voltage, transfer its gating charges through the transmembrane electric field, and exchange ion-pair partners between the INC and ENC [23] [17]. Comparison of the structures of Na_VAb and Na_VRh provides a snapshot of this transmembrane movement, as the S4 segment in Na_VRh has moved farther outward, such that its fourth gating charge is located above the HCS (Figure 3)[11]. A similar sliding-helix motion is observed during

activation of a voltage-sensitive phosphatase [28]. Most X-ray crystallographic structures of voltage sensors reveal part or all of the S4 segment in a 3_{10} rather than α-helical conformation [9-11]. These results raise the possibility that S4 may undergo a transition from α-helical to 3_{10} helical conformation during activation, which would allow outward movement of gating charges and exchange of ion pair partners with less rotation of the helix core [17, 23]. This outward movement of the gating charges in the VSM is coupled to pore opening and inactivation as described in the following sections.

Fast and slow inactivation

Mammalian Na_V channels are inactivated by both fast and slow processes, which involve distinct mechanisms and recover on very different time scales. Na_V channels in nerve and muscle open in response to depolarization and then inactivate within 1-2 ms [29]. This classical fast inactivation process is required for repetitive firing of action potentials in neural circuits and for controlling excitability in nerve and muscle cells, and it recovers within a few milliseconds upon repolarization. The short intracellular loop connecting homologous domains III and IV of the eukaryotic Na_V channel α subunit mediates fast inactivation by folding into the intracellular mouth of the pore and blocking it (Figure 1a; [5]). Bacterial Na_V channels lack such a fast inactivation gate, but they have a slow inactivation process.

Slow inactivation increases during trains of action potentials over hundreds of milliseconds and reverses even more slowly [30, 31]. Structure-function studies of mammalian Na_V channels suggested that the ion selectivity filter and the pore-lining S6 segments move during slow inactivation [30], which is corroborated by structure-function studies of the slow inactivation process of bacterial Na_V channels [32-34]. The Na_VAb-WT and Na_VRh structures revealed a distorted selectivity filter and a dramatic breakdown of the four-fold symmetry around the central axis (Figure 4) [10, 11], suggesting they represent the slow-inactivated state, which is the most stable functional state at the membrane potential of 0 mV in a protein crystal. In contrast to the original Na_VAb-I217C structure [9], these potentially slow-inactivated channels have partially collapsed pore domains, such that two S6 segments and P loops have moved toward the central axis of the pore and two have moved away [10, 11]. It is likely that this structural change underlies slow inactivation of Na_V channels in both prokaryotes and eukaryotes. Moreover, because voltage-dependent inactivation of Ca_V channels occurs on the same time scale as slow inactivation of Na_V channels, it is plausible that it involves a similar structural mechanism, as revealed in the ancestral Na_V channels from which both eukaryotic Na_V and Ca_V channels evolved. These structural studies revealed much about the mechanisms of opening and inactivation of the pores of Na_V and Ca_V channels. The following section considers how the open pores can rapidly and selectively conduct Na^+ or Ca^{2+}.

Structural basis for Na^+ conductance and selectivity

The four available crystal structures of NaChBac family members share a highly similar selectivity filter, which forms the narrowest constriction in the extracellular half of their pore. The prototypical Na_VAb selectivity filter is made of a short loop flanked by two short

helices, the P helix and P2 helix, which are connected to the S5 and S6 helix, respectively (Figure 2c) [9]. Classic studies of eukaryotic Na_V channels depicted a selectivity filter with an oxygen-lined pore about 3 Å by 5 Å in cross section [1, 35-37]. An ionized carboxylic group was proposed to serve as a high-field-strength (HFS) site, which can displace tightly bound waters of hydration and interact with Na^+ in a partially hydrated form. According to Eisenman's theory [1], such an anionic site favors small cations and confers Na^+ selectivity. This hallmark HFS site can be readily identified at the extracellular opening of the Na_VAb selectivity filter, where four Glu residues from the four subunits create a constriction with dimensions of 4.6 Å × 4.6 Å (Figure 4, 5a). The size of the orifice is just sufficient for Na^+ to go through together with at least two water molecules in the same plane, and possibly two additional ones "behind" and "in front" of the ion. Further into the conduction pathway, the Na_VAb selectivity filter features two additional central and inner sites, which are formed by two quartets of backbone carbonyls (Figure 5b). The symmetric geometry and nearby electron density of these two sites indicate that they could coordinate four planar water molecules around the pore axis to fully hydrate Na^+.

Other bacterial Na_V channel structures also revealed an aqueous selectivity filter with a wide lumen, an HFS site formed by Glu side chains, and two central and inner sites formed by backbone carbonyls [11, 15, 38]. Although the selectivity filter of Na_VAb was empty in the crystal, an island of electron density was found in the selectivity filters of both Na_VRh and Na_VMs [11, 38]. In the case of Na_VRh, crystallographic analysis assigned the density as a blocking Ca^{2+} ion in a mostly hydrated form [38]. A similarly hydrated ion has also been observed at an outer site in the extracellular vestibule of the Na_VAe1 and Na_VAb selectivity filters [9, 11]. This site could represent the entry point for permeant ions ready to be partially dehydrated.

While higher resolution structures of bacterial Na_V channels will be needed to better delineate the binding mode of hydrated Na^+, the overall features of their selectivity filters are in full agreement with the classical four-barrier, three-site model proposed for the asymmetric four-domain eukaryotic Na_V channels [37]. The size and chemical nature of the prokaryotic and eukaryotic Na_V channel selectivity filters are in stark contrast to K^+ channels, which select K^+ by completely removing its hydration shell through interaction with a much narrower array of backbone carbonyl oxygen atoms in the absence of negatively charged coordinating ligands (Figure 5c)[39]. Evidently, two fundamentally different modes of ion conductance and selectivity had evolved in bacterial Na^+ and K^+ channels, long before four-domain Na_V channels arose through evolution in eukaryotes.

Molecular dynamics of Na^+ permeation

The structure of bacterial Na_V channels provided crystallographic snapshots of the pore structure, but the chemical details of their ion permeation mechanism can be better understood through molecular dynamics simulations. A single open Na_V channel conducts ~10^7 Na^+ per second, with greater than 10-fold selectivity over K^+ and nearly 50-fold selectivity over Ca^{2+} [1]. This high rate of conductance precludes high-affinity binding because the residence time of each ion in the pore would be too long. The similarity in size of these ions also precludes ion-sieving as the primary mechanism of selectivity. How are

high rates of permeation and high ion selectivity achieved without high-affinity binding and molecular sieving?

Long, unbiased molecular dynamics simulations were carried out for Na_VAb at 0 mV, approximately the peak of Na^+ conductance during an action potential. More than 200 Na^+ ions passed inward through the ion selectivity filter at 6×10^6 per second and reached equilibrium across it [40]. As inward-moving Na^+ approaches the HFS site, molecular simulations revealed dynamic interactions between the carboxylates and Na^+, such that 1-3 waters of hydration in the inner shell were displaced by interaction with 1-3 carboxylates [40]. Upon binding Na^+, the carboxylates bend (or "dunk") deeper into the pore by rotating around a single torsion angle in the Glu side chains (Figure 5d). As they move inward past the HFS site, Na^+ ions regain a complete inner shell of water during interaction with the central and inner coordination sites formed by backbone carbonyls of Leu and Thr residues [40]. The primary sites of interaction during conductance were the carboxylates of the HFS site alone and combined interaction with the HFS site and the backbone carbonyls of Leu in the central site (Figure 5e). These molecular dynamics results reveal active catalysis of Na^+ conductance by correlated dunking movements of the Glu side chains. This novel feature of the HFS site in the selectivity filter, and the interactions with backbone carbonyls, are both essential steps in the ion permeation process.

Molecular dynamics simulations of Na_VMs and Na_VRh for shorter times at large negative and positive membrane potentials provide complementary views of the permeation process. Movement of multiple Na^+ ions was required for effective conductance, and two to three sites of interaction within the selectivity filter involving the HFS site and the Leu backbone carbonyls were observed [38, 41], consistent with the unbiased simulations [40]. Glu dunking was observed in some studies, but large negative membrane potentials might have reduced the extent of dunking observed [38] due to electrostatic repulsion of carboxylates by the negative internal membrane potential. Overall, molecular dynamics simulations performed in different ways give a generally consistent view of Na^+ conductance in bacterial Na_V channels.

From Na_VAb to Ca_VAb: structural insight into Ca^{2+} selectivity

Ca_V channels have evolved a selectivity mechanism that allows them to discriminate Ca^{2+} over the similar-sized Na^+, even though the latter is far more abundant in the extracellular solution. How can Ca_V channels achieve this high ion selectivity while maintaining high-throughput conductance? At the sequence level, Ca_V channels are closely related to Na_V channels, whose ion selectivity can be altered to favor Ca^{2+} with simple mutations in the selectivity filter [42-44]. Inspired by early work converting NaChBac to a Ca^{2+}-selective form with such mutations [45], crystallographic analysis of a similarly engineered Na_VAb mutant, known as Ca_VAb, has provided valuable structural insights into Ca^{2+} selectivity and permeation in Ca_V channels [46].

Ca_VAb was created by substituting three amino acid residues in the ion selectivity filter of Na_VAb (including the HFS site Glu) with Asp (Figure 6a; TLESWSM to TLDDWSD). These substitutions confer Ca^{2+} selectivity with a permeability ratio of $P_{Ca}:P_{Na}$~400:1,

equivalent to mammalian Ca_V channels. The crystal structure of Ca_VAb revealed little conformational change in the backbone geometry of the selectivity filter, indicating that ion selectivity is exclusively dictated by the amino acid side chains (Figure 6a). Previous experimental and theoretical studies of mammalian Ca_V channels have postulated that Ca_V channels select Ca^{2+} over Na^+ on the basis of affinity and that the high flux of Ca^{2+} is mediated by a "knock-off" mechanism (see Glossary), in which a second Ca^{2+} entering the pore "knocks off" a previous resident Ca^{2+} by charge repulsion. However, this concept was inconsistent with the single high-affinity Ca^{2+}-binding site suggested by careful analyses of mutations and cation block [43]. With Ca^{2+} included in the crystallization medium, the Ca_VAb structure clearly revealed three ion-binding sites lining up along the axis of the selectivity filter (Figure 6b) [46]. Leading from the entry to the exit of the ion conduction pathway, these three sites are coordinated by a quartet of Asp residues (Site 1), a box of four Asp side chains and four backbone carbonyls of Leu residues (Site 2), and a quartet of backbone carbonyls of Thr residues alone (Site 3). The distances between all three ion-binding sites and their surrounding oxygen atoms suggest that Ca^{2+} is bound and conducted in hydrated form, in agreement with the 6 Å diameter estimated for the selectivity filter in mammalian Ca_V channels [47]. Favorable crystal structures revealed waters of hydration surrounding Ca^{2+} ions [46]. By titrating Ca^{2+} concentration, the central site of Ca_VAb was identified as the high affinity site, whereas the third site close to the central cavity showed lowest affinity [46]. Consistent with studies of mammalian Ca_V channels, divalent cations such as Cd^{2+} and Mn^{2+} block Ca_VAb by occupying only the central high-affinity site [46].

The spatial relationships among the three Ca^{2+}-binding sites in the multi-ion pore of Ca_VAb and their relative affinities for Ca^{2+} point to an ion conductance mode that combines the "knock-off" mechanism [48-50] and a stepwise-permeation model (see Glossary) [51, 52] in which conducted Ca^{2+} moves in steps from an external low affinity binding site to high affinity sites in the selectivity filter and back to low affinity sites in the central cavity. In the Ca_VAb selectivity filter, the three Ca^{2+}-binding sites are separated by a distance of ~4.5 Å, which would trigger electrical repulsion between Ca^{2+} ions. The combination of the central high-affinity site with outer and inner sites of lower affinity provides potential energy steps to facilitate the entry and exit of Ca^{2+} ions transiting the selectivity filter. In the presence of extracellular Ca^{2+} in high concentration, these two mechanisms could allow the selectivity filter to oscillate between a single-ion bound state with the high-affinity central site occupied and a two-ion bound state with central site empty, thereby achieving a high unidirectional Ca^{2+} flux (Figure 6c). Although Ca_VAb is engineered from Na_VAb and does not contain a selectivity filter identical to that of the mammalian Ca_Vs, it has very similar ion selectivity to a voltage-gated Ca_V channel. The basic principles governing Ca^{2+} conductance by Ca_VAb are most likely shared by the mammalian channels.

Concluding remarks

Structural studies of the bacterial Na_V channels have given an unexpected wealth of new insights into ion channel function at molecular, mechanistic, and even atomic levels. The structures of Na_VAb and Ca_VAb and the related molecular dynamics simulations revealed the mechanism of highly selective conductance of hydrated cations in the voltage-gated ion channel family. Ion selectivity is generated by interaction with the inner shell of waters of

hydration rather than by direct interactions with the dehydrated ion itself, and molecular sieving based on ion size plays little role in the selectivity process. Glu side chains accompany conducted Na^+ ions in a dunking motion. The structures of the VSMs of Na_VAb and other bacterial Na_V channels in the activated conformation and the structural models of the VSM of NaChBac in resting and activated states have given much-needed new definition to the mechanism of voltage sensor function. The nature of the conformational changes during slow inactivation have been revealed by the structures of wild-type Na_VAb and Na_VRh, which likely are good models for slow inactivation of eukaryotic Na_V channels and voltage-dependent inactivation of eukaryotic Ca_V channels. With many questions to be addressed by future studies (see Outstanding Question Box), the new knowledge of these fundamental processes that underlie electrical signaling will have important implications for the many diseases caused by altered ion channel function [53] and for development of new generations of drugs targeted to specific ion channel subtypes [54].

Acknowledgements

W.A.C. and N.Z. are supported by NIH grants R01HL12808 and R01HL17896. W.A.C. is also supported by NIH grant R01NS15751. N.Z. is a Howard Hughes Medical Institute investigator.

Glossary

Depolarization	A rapid shift of the charge inside the cell from negative to neutral or positive.
Resting state	The state of a Na_V or Ca_V channel under resting membrane potential. The resting state of the channel is characterized by a closed pore with low open probability and the S4 segments of the VSMs in inward, resting positions.
Activated state	The state of a Na_V or Ca_V channel during membrane depolarization. The channel is characterized by an open pore and the S4 segments of the VSMs in outward, activated positions.
Pre-open state	A transitional state of a Na_V or Ca_V channel under membrane depolarization. This state is characterized by activated VSMs with the S4 helix in outward, activated positions with the pore still closed, but poised to spring open.
Inactivated state	The state adopted by a Na_V or Ca_V channel during prolonged depolarization. Inactivated states are characterized by one or more VSMs in activated conformation but a blocked pore.
Fast inactivation	Rapid inactivation of eukaryotic Na_V channels within 1-2 milliseconds. The inactivation process involves a hinged-lid mechanism in which the pore is plugged by the intracellular linker between domains III and IV. This structural feature is not present in bacterial Na_V channels. Fast inactivation is rapidly reversed with a few milliseconds upon repolarization.

Slow inactivation	Slow inactivation of both prokaryotic and eukaryotic Na_V channels over hundreds of milliseconds. The inactivation mechanism involves rearrangement of the pore. Slow inactivation is slowly reversed upon repolarization. Voltage-dependent inactivation of eukaryotic Ca_V channels is likely to share a similar mechanistic and structural basis.
Selectivity filter	A constriction of an ion channel in the pore, which confers selective permeation of specific ions by the channel.
Voltage-sensing module	A four transmembrane helical module that confers voltage sensitivity to voltage-gated ion channels.
Gating charges	Positively charged amino acid residues (usually Arg) located at three-residue intervals along the S4 transmembrane segment in the VSM. The electrical field caused by the membrane potential exerts an electrostatic force on these positive charges. At the negative internal resting membrane potential, these positive gating charges are pulled inward, like the trigger of a cocked gun. Depolarization releases this electrostatic force, allowing the gating charges and the S4 segment to move outward rapidly, activate the VSM, and initiate the conformational changes that open the pore. Repolarization pulls the gating charges back into their inward, resting position where they are ready for activation again upon depolarization.
Pore module	The S5 and S 6 transmembrane segments and intervening P loop that form the central pore of a voltage-gated ion channel where permeating ions are conducted.
Activation gate	A structural element at the intracellular end of a voltage-gated ion channel that controls the opening and closure of the pore in response to VSM activation.
“Knock-off” mechanism	A hypothetical ion conductance mechanism in which ionic repulsion triggered by simultaneous occupation of adjacent ion-binding sites facilitates the rapid and unidirectional movement of ions through the selectivity filter.
Stepwise permeation	A rate-theory based ion permeation mechanism for Ca_V channel in which stepwise changes in the binding affinities of Ca^{2+} ions to multiple sites of the selectivity filter facilitate the high Ca^{2+} flux without repulsive interactions. The energy barriers are lower, and therefore conduction rates are faster, for stepwise movement from free solution to high-affinity ion binding sites than for a single jump from free solution to a high-affinity ion binding site.

REFERENCES

1. Hille, B. Ionic Channels of Excitable Membranes. 3rd Ed. Sinauer Associates Inc.; Sunderland, MA: 2001.

2. Tsien RW. Calcium channels in excitable cell membranes. Annu Rev Physiol. 1983; 45:341–358. [PubMed: 6303205]
3. Catterall WA. Voltage-gated calcium channels. Cold Spring Harb Perspect Biol. 2011; 3:a003947. [PubMed: 21746798]
4. Catterall WA. The molecular basis of neuronal excitability. Science. 1984; 223:653–661. [PubMed: 6320365]
5. Catterall WA. From ionic currents to molecular mechanisms: The structure and function of voltage-gated sodium channels. Neuron. 2000; 26:13–25. [PubMed: 10798388]
6. Stühmer W. Structure-function studies of voltage-gated ion channels. Annu Rev Biophys Biophys Chem. 1991; 20:65–78. [PubMed: 1714280]
7. Yu FH, Catterall WA. The VGL-chanome: a protein superfamily specialized for electrical signaling and ionic homeostasis. Sci STKE. 2004; 2004:re15. [PubMed: 15467096]
8. Ren D, et al. A prokaryotic voltage-gated sodium channel. Science. 2001; 294:2372–2375. [PubMed: 11743207]
9. Payandeh J, et al. The crystal structure of a voltage-gated sodium channel. Nature. 2011; 475:353–358. [PubMed: 21743477]
10. Payandeh J, et al. Crystal structure of a voltage-gated sodium channel in two potentially inactivated states. Nature. 2012; 486:135–139. [PubMed: 22678296]
11. Zhang X, et al. Crystal structure of an orthologue of the NaChBac voltage-gated sodium channel. Nature. 2012; 486:130–134. [PubMed: 22678295]
12. Tsai CJ, et al. Two alternative conformations of a voltage-gated sodium channel. J Mol Biol. 2013; 425:4074–4088. [PubMed: 23831224]
13. McCusker EC, et al. Structure of a bacterial voltage-gated sodium channel pore reveals mechanisms of opening and closing. Nat Commun. 2012; 3:1102. [PubMed: 23033078]
14. Shaya D, et al. Voltage-gated sodium channel (Na_V) protein dissection creates a set of functional pore-only proteins. Proc Natl Acad Sci U S A. 2011; 108:12313–12318. [PubMed: 21746903]
15. Shaya D, et al. Structure of a prokaryotic sodium channel pore reveals essential gating elements and an outer ion binding site common to eukaryotic channels. J Mol Biol. 2014; 426:467–483. [PubMed: 24120938]
16. Bagneris C, et al. Structural model of the open-closed-inactivated cycle of prokaryotic voltage-gated sodium channels. J Gen Physiol. 2015; 145:5–16. [PubMed: 25512599]
17. Yarov-Yarovoy V, et al. Structural basis for gating charge movement in the voltage sensor of a sodium channel. Proc Natl Acad Sci U S A. 2012; 109:E93–102. [PubMed: 22160714]
18. Bagneris C, et al. Role of the C-terminal domain in the structure and function of tetrameric sodium channels. Nat Commun. 2013; 4:2465. [PubMed: 24051986]
19. Irie K, et al. The C-terminal helical bundle of the tetrameric prokaryotic sodium channel accelerates the inactivation rate. Nat Commun. 2012; 3:793. [PubMed: 22531178]
20. Armstrong CM, Bezanilla F. Currents related to movement of the gating particles of the sodium channels. Nature. 1973; 242:459–461. [PubMed: 4700900]
21. Bezanilla F. The voltage sensor in voltage-dependent ion channels. Physiol Rev. 2000; 80:555–592. [PubMed: 10747201]
22. Yarov-Yarovoy V, et al. Voltage sensor conformations in the open and closed states in ROSETTA structural models of K^+ channels. Proc Natl Acad Sci U S A. 2006; 103:7292–7297. [PubMed: 16648251]
23. Catterall WA. Ion channel voltage sensors: structure, function, and pathophysiology. Neuron. 2010; 67:915–928. [PubMed: 20869590]
24. Vargas E, et al. An emerging consensus on voltage-dependent gating from computational modeling and molecular dynamics simulations. J Gen Physiol. 2012; 140:587–594. [PubMed: 23183694]
25. Long SB, et al. Voltage sensor of Kv1.2: structural basis of electromechanical coupling. Science. 2005; 309:903–908. [PubMed: 16002579]
26. Long SB, et al. Crystal structure of a mammalian voltage-dependent Shaker family K^+ channel. Science. 2005; 309:897–903. [PubMed: 16002581]

27. Long SB, et al. Atomic structure of a voltage-dependent K^+ channel in a lipid membrane-like environment. Nature. 2007; 450:376–382. [PubMed: 18004376]
28. Li Q, et al. Structural mechanism of voltage-dependent gating in an isolated voltage-sensing domain. Nat Struct Mol Biol. 2014; 21:244–252. [PubMed: 24487958]
29. Hodgkin AL, Huxley AF. The dual effect of membrane potential on sodium conductance in the giant axon of Loligo. J Physiol. 1952; 116:497–506. [PubMed: 14946715]
30. Vilin YY, Ruben PC. Slow inactivation in voltage-gated sodium channels: molecular substrates and contributions to channelopathies. Cell Biochem Biophys. 2001; 35:171–190. [PubMed: 11892790]
31. Rudy B. Slow inactivation of the sodium conductance in squid giant axons. Pronase resistance. J Physiol. 1978; 283:1–21. [PubMed: 722569]
32. Zhao Y, et al. A gating hinge in Na^+ channels; a molecular switch for electrical signaling. Neuron. 2004; 41:859–865. [PubMed: 15046719]
33. Pavlov E, et al. The pore, not cytoplasmic domains, underlies inactivation in a prokaryotic sodium channel. Biophys J. 2005; 89:232–242. [PubMed: 15849254]
34. Zhao Y, et al. Reversed voltage-dependent gating of a bacterial sodium channel with proline substitutions in the S6 transmembrane segment. Proc Natl Acad Sci U S A. 2004; 101:17873–17878. [PubMed: 15583130]
35. Hille B. The permeability of the sodium channel to organic cations in myelinated nerve. J Gen Physiol. 1971; 59:599–619. [PubMed: 5315827]
36. Hille B. The permeability of the sodium channel to metal cations in myelinated nerve. J Gen Physiol. 1972; 59:637–658. [PubMed: 5025743]
37. Hille B. Ionic selectivity, saturation, and block in sodium channels. A four-barrier model. J Gen Physiol. 1975; 66:535–560. [PubMed: 1194886]
38. Ulmschneider MB, et al. Molecular dynamics of ion transport through the open conformation of a bacterial voltage-gated sodium channel. Proc Natl Acad Sci U S A. 2013; 110:6364–6369. [PubMed: 23542377]
39. Zhou Y, et al. Chemistry of ion coordination and hydration revealed by a potassium channel- Fab complex at 2.0 A resolution. Nature. 2001; 414:43–48. [PubMed: 11689936]
40. Chakrabarti N, et al. Catalysis of Na^+ permeation in the bacterial sodium channel Na_VAb. Proc Natl Acad Sci U S A. 2013; 110:11331–11336. [PubMed: 23803856]
41. Zhang X, et al. Analysis of the selectivity filter of the voltage-gated sodium channel Na_VRh. Cell Res. 2013; 23:409–422. [PubMed: 23247626]
42. Heinemann SH, et al. Calcium channel characteristics conferred on the sodium channel by single mutations. Nature. 1992; 356:441–443. [PubMed: 1313551]
43. Ellinor PT, et al. Ca^{2+} channel selectivity at a single locus for high-affinity Ca^{2+} interactions. Neuron. 1995; 15:1121–1132. [PubMed: 7576655]
44. Yang J, et al. Molecular determinants of Ca^{2+} selectivity and ion permeation in L-type Ca^{2+} channels. Nature. 1993; 366:158–161. [PubMed: 8232554]
45. Yue L, et al. The cation selectivity filter of the bacterial sodium channel, NaChBac. J Gen Physiol. 2002; 120:845–853. [PubMed: 12451053]
46. Tang L, et al. Structural basis for Ca^{2+} selectivity of a voltage-gated calcium channel. Nature. 2014; 505:56–61. [PubMed: 24270805]
47. Mccleskey EW, Almers W. The Ca Channel in Skeletal-Muscle Is a Large Pore. Proc Nat Acad Sci U S A. 1985; 82:7149–7153.
48. Almers W, McCleskey EW. The nonselective conductance due to calcium channels in frog muscle: calcium-selectivity in a single file pore. J Physiol. 1984; 353:585–608. [PubMed: 6090646]
49. Almers W, et al. A nonselective cation conductance in frog muscle membrane blocked by micromolar external Ca++ J Physiol. 1984; 353:565–583. [PubMed: 6090645]
50. Hess P, Tsien RW. Mechanism of ion permeation through calcium channels. Nature. 1984; 309:453–456. [PubMed: 6328315]
51. Dang TX, McCleskey EW. Ion channel selectivity through stepwise changes in binding affinity. J Gen Physiol. 1998; 111:185–193. [PubMed: 9450938]

52. Sather WA, McCleskey EW. Permeation and selectivity in calcium channels. Annu Rev Physiol. 2003; 65:133–159. [PubMed: 12471162]

53. Ashcroft, FM. Ion Channels and Disease. Academic Press; London: 2000.

54. Cox, B.; Gosling, M. Ion Channel Drug Discovery. Royal Society of Chemistry; 2014.

55. Bagneris C, et al. Prokaryotic NavMs channel as a structural and functional model for eukaryotic sodium channel antagonism. Proc Natl Acad Sci U S A. 2014; 111:8428–8433. [PubMed: 24850863]

56. Catterall WA, Swanson TM. Structural Basis for Pharmacology of Voltage-Gated Sodium and Calcium Channels. Mol Pharmacol. 2015; 88:141–150. [PubMed: 25848093]

Outstanding Questions Box

1. What is the structural basis of the resting state of a Na_V (or Ca_V) channel?

So far, the available bacterial Na_V channel structures (Na_VAb and Na_VRh) have only captured the VSMs in their activated states, in which the S4 helices have already undergone substantial outward movement. The structure of the resting state of a bacterial Na_V channel, in which the VSM is expected to have a distinct conformation with the gating charges on the intracellular side of the HCS, remains to be determined.

2. How does VSM activation lead to pore opening?

In voltage-gated ion channels, the VSM is believed to control the activation gate of the pore module via the S4-S5 linker. The structural mechanism underlying this allosteric regulation, however, remains elusive.

3. Can we use the prokaryotic channels to investigate drug binding?

One of the interesting properties of the prokaryotic Na_V channels is their pharmacological sensitivity to eukaryotic Na_V and Ca_V channel blockers [8]. A recent structural study of Na_VMs has provided evidence for drug binding at the central cavity of its pore module[55]. Future structural studies of other NaChBac family members might reveal more detailed drug-channel interactions (see ([56]) for review).

4. How do the four-domain asymmetric eukaryotic Nav and Cav channels work?

While the bacterial Na_V channel structures help to elucidate some fundamental principles of Na_V and Ca_V channel functions, the eukaryotic Na_V and Ca_V channels have a far more complex architecture and regulatory mechanisms. Structural determination of the eukaryotic Na_V and Ca_V channels remains a “Holy Grail” of ion channel research.

Highlights

- Prokaryotic ancestors provide insights into voltage-gated Na^+ and Ca^{2+} channels.
- Voltage-gated Na^+ channels permeate sodium ions in a partially hydrated form.
- Slow inactivation of Na^+ channels likely involves partial collapse of the pore.
- New data support the *sliding helix* model for voltage-dependent gating.
- Structural basis of Ca^{2+} selectivity and conductance by Ca^{2+}-selective mutants.

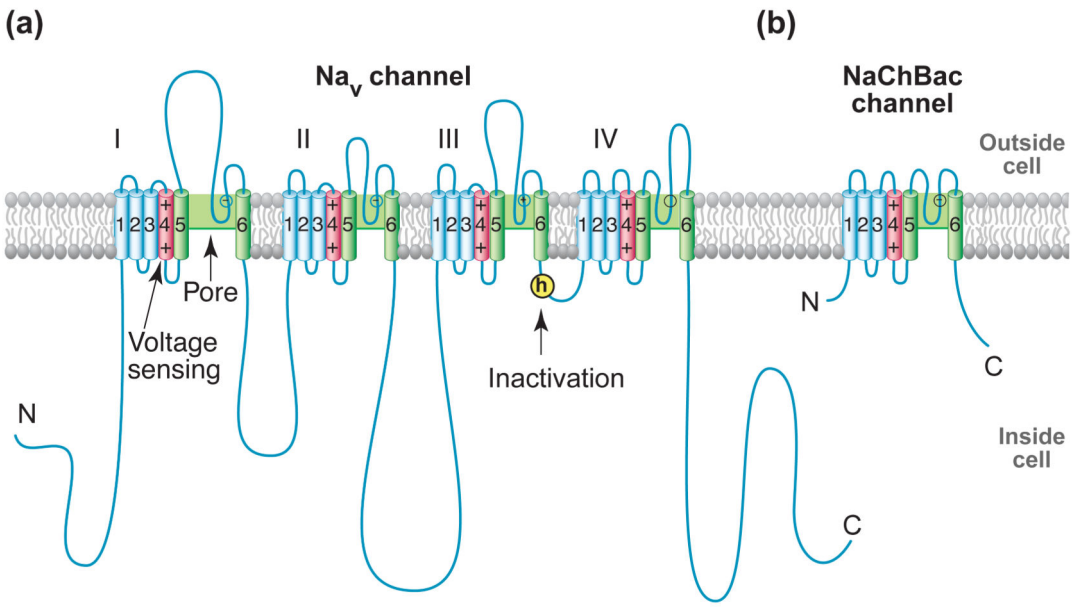

Figure 1. Na$_V$ Channel Structure

(a) Two-dimensional schematic map of Na$_V$ channel structure and function. The α subunit of Na$_V$1.2 channels is illustrated as a transmembrane folding diagram in which cylinders represent transmembrane alpha helices and lines represent connecting amino acid sequences in proportion to their length. The roman numerals indicate the four homologous domains and the Arabic numerals are used to label the six transmembrane helices. The S4 helices are colored in red with "+" signs indicating gating charges. The S5-S5 helices are colored in green and the small white circles indicate key residues in the selectivity filter with "+" and "–" signs indicating their charge states. The yellow circle with an "h" indicates inactivation gate. **(b)** Schematic map of the bacterial NaChBac channel, which contains the minimal functional elements of a single homologous domain in a mammalian Na$_V$ channel.

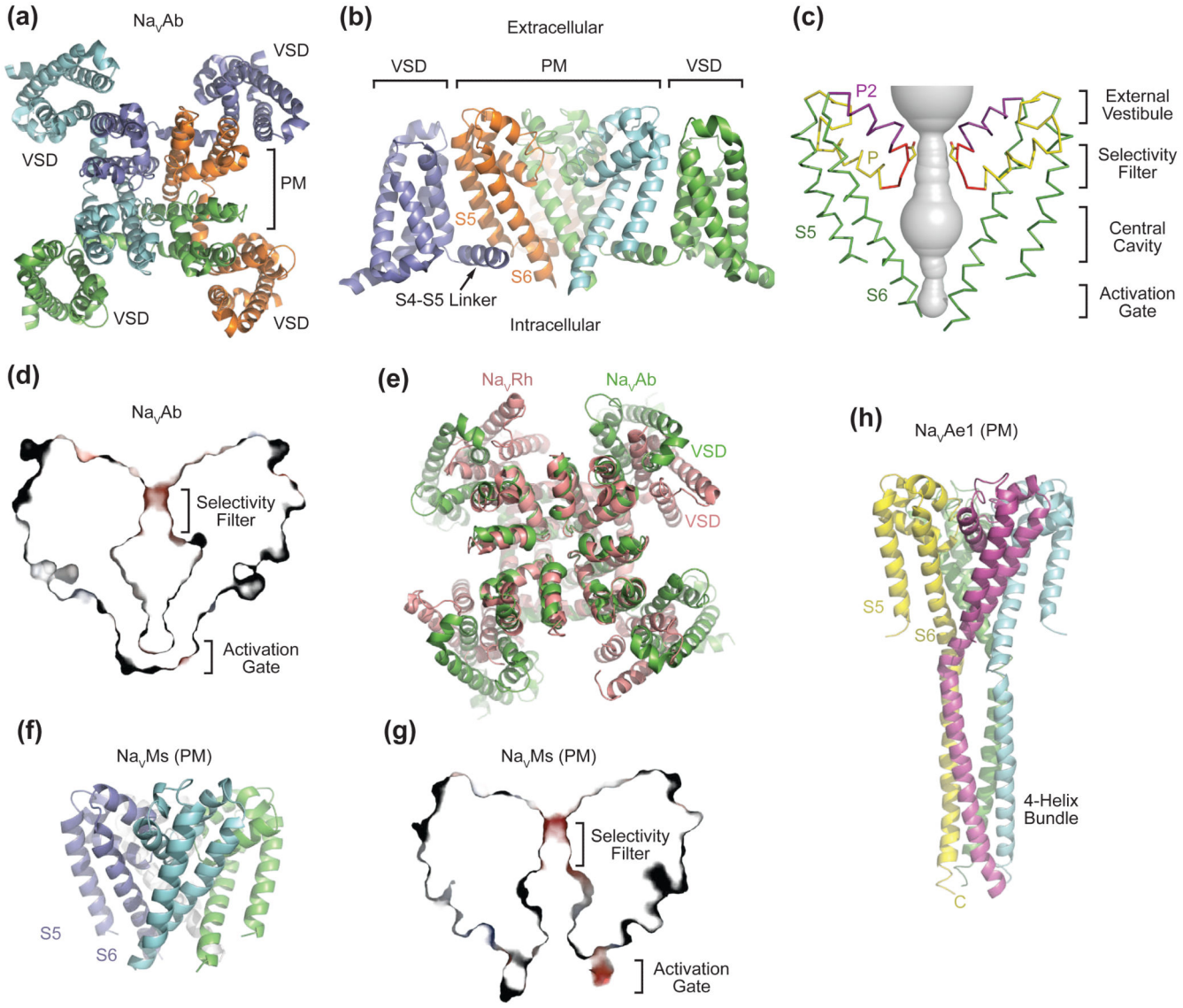

Figure 2. Overall Structures of Prokaryotic Na_V Channels

(a) Structure of the Na_VAb bacterial Na_V channel determined at 2.7Å resolution and viewed from the extracellular side [9]. The four subunits of the homotetrameric channel are shown in different colors. The central pore is surrounded by four VSMs. **(b)** Side view of Na_VAb with the same coloring scheme as shown in (a). S5 and S6 helices of one subunit (slate) and the VSM of another subunit (cyan) are omitted for clarity. **(c)** Architecture of the Na_VAb pore with pore volume shown in grey and the high-strength-field (HSF) site residue Glu177 shown in sticks. P and P2 indicate the P and P2 helices. **(d)** Cross-section of the Na_VAb pore showing the closed activation gate. The selectivity filter is shown with electrostatic surface potential colored from −50 to 50 kT (red to blue). **(e)** Superposition of Na_VRh and Na_VAb with their PMs superimposed [9, 11]. The VSM of the two channels packs against the PM at different angles. (**f**) Structure of the Na_VMs pore module [13]. **(g)** Cross-section of the Na_VMs pore showing the open conformation of its activation gate [18]. The selectivity filter

is shown with electrostatic surface potential colored from −50 to 50 kT (red to blue). **(h)** Structure of the Na_VAe1 pore with well-resolved C-terminal domain forming a four-helix bundle [15].

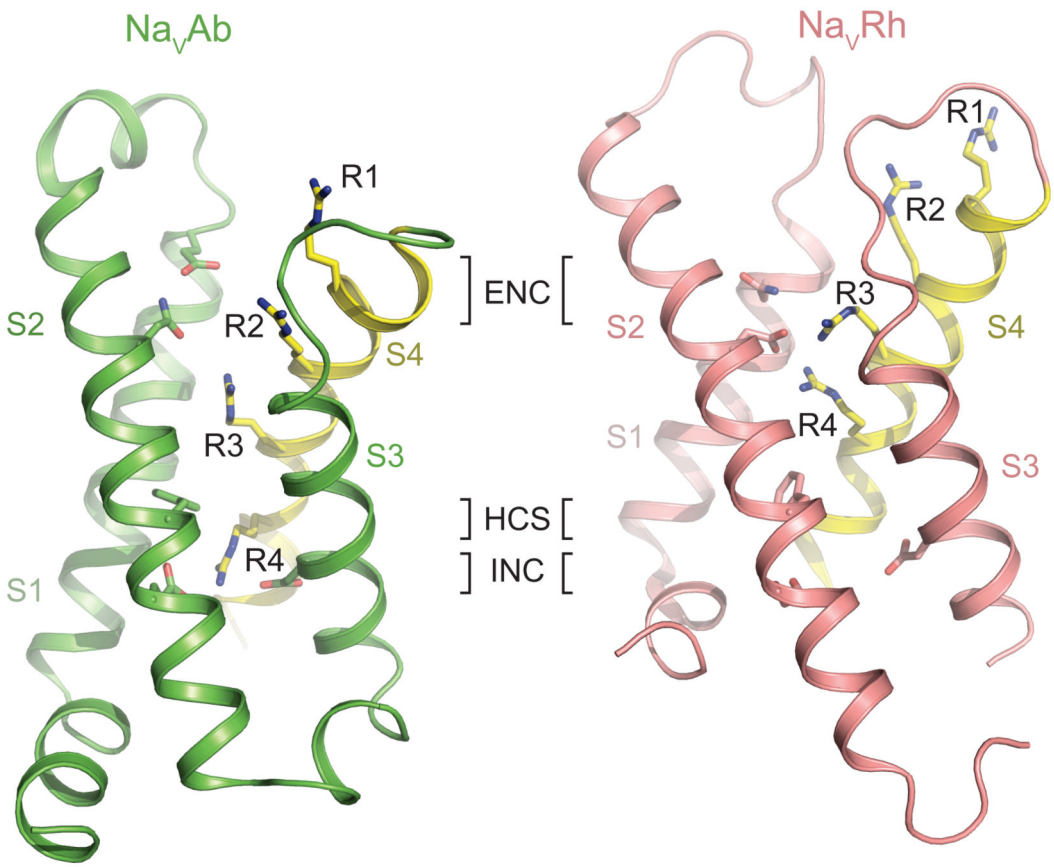

Figure 3. A Comparison of the Voltage-sensor Domains of Na_VAb and Na_VRh

The VSMs of Na_VAb (left, green) and Na_VRh (right, salmon) are shown in ribbon diagram [9, 11]. The sliding S4 helix is highlighted in yellow with the side chains of the four gating charge arginine residues (R1-R4) shown in sticks. Key residues forming the extracellular negative cluster (ENC), intracellular negative cluster (INC), and hydrophobic constriction site (HCS) are shown in sticks. The R4 residue of Na_VAb and Na_VRh interacts with the INC and ENC residues, respectively.

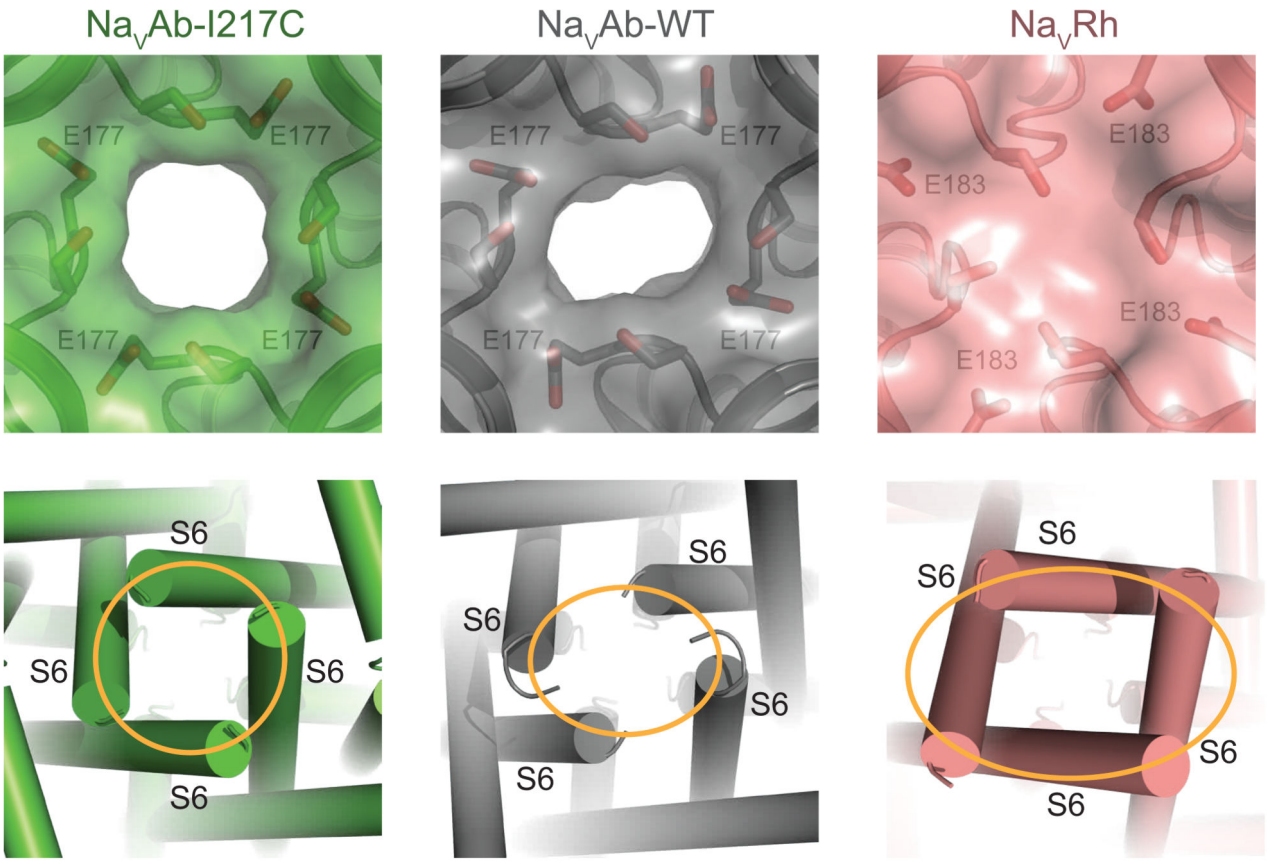

Figure 4. Structural Basis of Slow Inactivation

Specific structural features of Na_VAb-WT and Na_VRh, including a distorted selectivity filter and the breakdown of the four-fold symmetry of the pore, as expected for the slow inactivation state. Top panel: Close-up views of the extracellular entrance of Na_VAb-I217C (green, symmetric), Na_VAb-WT (grey, asymmetric), and Na_VRh (salmon, collapsed) with semi-transparent surface representation of the three channels [9-11]. The high-strength-field site glutamate residue in each structure along with its nearby serine residue is shown in sticks. Bottom panel: Close-up view of the intracellular closed activation gate of Na_VAb-I217C (symmetric, orange circle), Na_VAb-WT (asymmetric, orange oval), and Na_VRh (asymmetric, orange oval). .

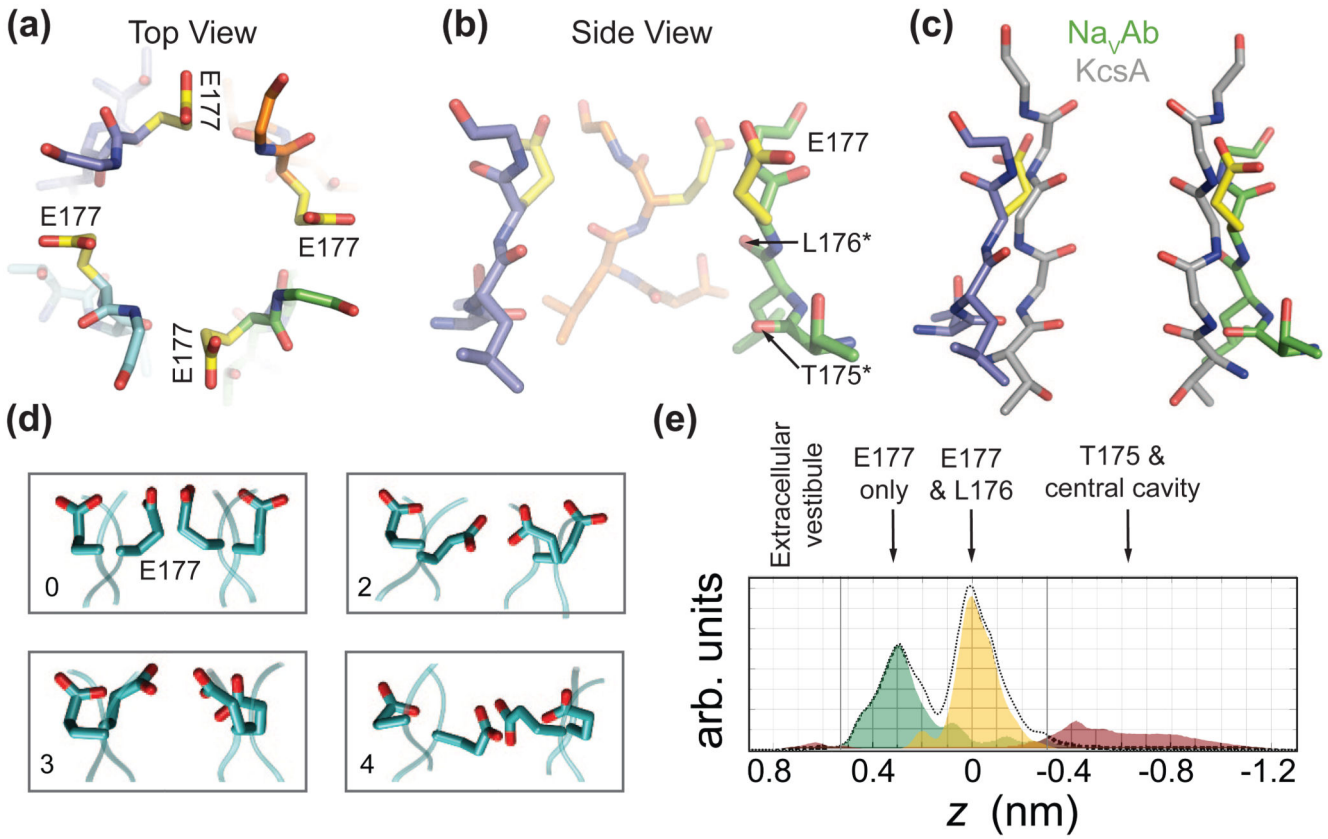

Figure 5. Selectivity Filter of Na_VAb

(a) Close-up view of the extracellular entrance of Na_VAb-I217C with the high-strength-field site, Glu177, highlighted in yellow [9]. **(b)** Side view of the Na_VAb-I217C selectivity filter showing Glu177 (yellow) and the backbone carbonyls of Leu176 and Thr175, all of which are involved in selecting and permeating partially hydrated sodium ions. **(c)** Superposition of Na_VAb and a K^+-channel (PDB code 1K4C) selectivity filter. The structural alignment, which is based on the common P-helices of the two channels, highlights the significant differences in the width of the two selectivity filters. **(d)** Different conformational states of the four high-strength-field site Glu177 residues captured in equilibrium molecular dynamics simulation of Na_VAb in a hydrated lipid bilayer with Na^+ moving in and out of the pore [40]. The side chains of Glu177 point either out toward the mouth of the selectivity filter or into the lumen (0-4 indicate the number of Glu side chains dunked; Na^+ ions not shown). **(e)** Axial distribution of Na^+ atoms in the selectivity filter and central cavity of Na_VAb. Three distinguishable states are highlighted in which Na^+ is directly bound to Glu177 (green), to both Glu177 and the backbone carbonyl of Leu176 (yellow), or to neither (brown). **(d)** and **(e)** are adapted from reference [40].

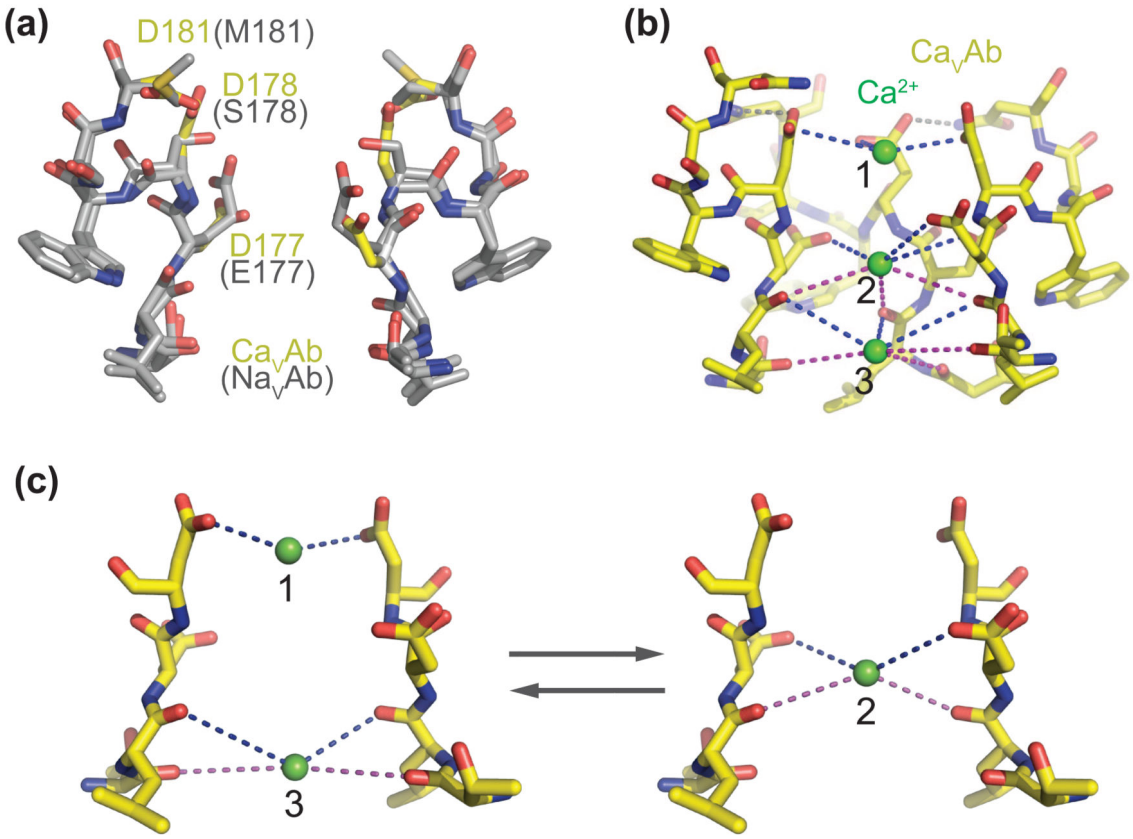

Figure 6. Ca^{2+} Selectivity and Permeation by Ca_VAb

(a) Side view of the superimposed selectivity filters of Ca_VAb and Na_VAb [9, 46]. The side chains of the three residues of Na_VAb mutated to generate Ca_VAb are colored in yellow in the Ca_VAb structure. The backbone structure of the selectivity filters of the two channels are nearly identical. **(b)** Side view of the Ca_VAb selectivity filter with three Ca^{2+} (green spheres) binding sites and their coordinating oxygen atoms. The distances between Ca^{2+} and the oxygen atoms indicated with dash lines range from 4.0 Å to 5.0 Å. **(c)** A proposed mechanism of Ca^{2+} permeation by Ca_VAb based on a combination of the “knock-out” and “stepwise permeation” models. The selectivity filter oscillates between two proposed ionic occupancy states where Ca^{2+} ions either bind to position 2, the high-affinity binding site, or position 1 and 3, which bind the ion at lower affinities.